Received: 28 April 2016 | Accepted: 8 August 2016

DOI: 10.1111/jace.14491

ORIGINAL ARTICLE

Journal of the American Ceramic Society

The influence of physical properties of ZnO films on the efficiency of planar ZnO/perovskite/P3HT solar cell

Zhiwen Qiu | Shuai Yuan | Haibo Gong | Hailiang Zhang | Xiaofeng Qiu | Ting Luo | Bingqiang Cao

Materials Research Center for Energy and Photoelectrochemical Conversion, School of Material Science and Engineering, University of Jinan, Jinan, Shandong, China

Correspondence
Bingqiang Cao, Materials Research Center for Energy and Photoelectrochemical Conversion, School of Material Science and Engineering, University of Jinan, Jinan, Shandong, China.
Email: mse_caobq@ujn.edu.cn

Funding information
NSFC, Grant/Award Number: 51472110, 11174112; Shandong Provincial Natural Science Foundation, Grant/Award Number: JQ201214, 2014ZRB01A47; postgraduate innovation project, Grant/Award Number: YCXB15001;

Abstract

ZnO thin films prepared by pulsed laser deposition at low temperature are utilized as the electron transport layer in $CH_3NH_3PbI_{3-x}Cl_x$-based perovskite solar cells with a planar heterojunction structure. Oxygen pressure greatly influences the transparent and conductive properties of ZnO films, which are extremely important as electron transport layer for the perovskite solar cells. The transparent and conductive properties of the films under different oxygen pressures are studied by ultraviolet-visible spectrophotometer and Hall effect measurement system. Through controlling the oxygen pressure, transparent ZnO films with high conductivity are grown and adopted as electron transport layer for planar perovskite solar cell with a power conversion efficiency of 6.3%. After further surface modification of ZnO electron transport layer with [6,6]-phenyl-C61-butyric acid methyl ester, the efficiency of the planar solar cell increases to 7.5%.

KEYWORDS
electron transport layer, oxygen pressure, perovskite solar cell, pulsed laser deposition, zinc oxide

1 | INTRODUCTION

Since organometal halide perovskite sensitized solar cells ($CH_3NH_3PbX_3$, X: Cl, Br, or I) were firstly reported by Miyasaka et al.,[1] a major scientific breakthrough in the field of photovoltaics has been the emergence of organometal perovskites as absorber materials, achieving exceptional progress in solar cell performance.[2] Typically, $CH_3NH_3PbI_3$ has a direct optical band gap of around 1.5 eV,[3] low exciton binding energy (~45 meV),[4] and apparent tolerance of structural defects, high optical absorption, and long charge carrier diffusion lengths.[5] So far, the most efficient perovskite solar cells with PCE over 15% have a typical planar P–i–N structure of HTL/perovskite/ETL. HTL represents the *p*-type hole transport layer, and ETL represents the *n*-type electron transport layer.[6-8] The ETL and HTL layers not only collect the currents but also block the holes and the electrons, respectively. They also prevent the perovskite active layer from the direct contact with electrodes to reduce recombination of photocurrent.[9] The film roughness of electron transport layer also influences the growth of perovskite layer, especially for its surface morphology. Moreover, the electrical and optical properties of ETLs can significantly affect the performance of perovskite solar cells in terms of fill factor (FF), open-circuit voltage (V_{oc}), and short-circuit current (J_{sc}). So, selecting ETL with controlled property is essential to understand the solar cell photovoltaic processes such as photocarriers separation, transport, extraction, and recombination.[10]

In a planar P–i–N perovskite solar cell, a metal oxide dense film, such as TiO_2[11,12] or ZnO[13,14] is usually used as an electron transport layer to beneficially transfer the electrons and block the holes. Although the highest efficiency was obtained with TiO_2 film-based perovskite solar cells,[15] ZnO is also very attractive owing to the following material characteristics. First, ZnO is a wide band semiconductor with similar band gap structure to that of TiO_2

but has higher electron mobility.[16-18] Importantly, high crystalline ZnO films can be grown at low temperature without sintering processes.[19] Several growth methods including sol-gel process, electrodeposition, and sputtering could be adopted for ZnO films.[20] For example, Park *et al*[21] prepared ZnO nanorod-based perovskite solar cell in the absence of a compact TiO_2 blocking layer with a power conversion efficiency (PCE) of 11.13%. However, high processing temperature (450°C) was adopted to anneal the ZnO nanorods. Kelly et al.[22] reported the use of ZnO nanoparticles thin film as ETL in a $CH_3NH_3PbI_3$-based solar cell without high-temperature sintering. But impurities can be easily introduced into ZnO nanoparticles by a solution method. Mahmood et al.[23] explored a double-layered ZnO film for mesoscopic perovskite thin film solar cell, showing PCE of 10.35%. The low-temperature grown ZnO film as electron transport layer in perovskite solar cells highlight the opportunities to further improve the efficiency by optimizing the ETL optical and electrical properties. For example, Song *et al*[24] adopted spin-coated ZnO thin film as electron transport layer and the layer thickness as a key parameter for the photovoltaic performance was optimized. Moreover, precise controlling the semiconductor property of ETL like its transparence and conductivity is very important for perovskite solar cells, yet there is a dearth of effort in this area. Only few reports discussed the effects of the nonstoichiometry defects of the metal oxide electron transport layer on the photovoltaic performance of the planar perovskite solar cell.[25] Therefore, we need to explore new method to grow electron transport layer in a controlled manner, and regulate their physical property.

Pulsed laser deposition (PLD) is now one of the most successful growth techniques to obtain high-quality oxide thin films and nanostructures.[26-28] In addition, although undoped ZnO is a typical *n*-type semiconductor, the growth environment, such as oxygen partial pressure, can greatly influence the transparent and conductive properties of ZnO film. In this regard, Carcia *et al*[29] stated that the resistivity of polycrystalline undoped ZnO films can be changed by more than 10 orders of magnitude by controlling the oxygen partial pressure with rf-magnetron sputtering. Further, it was also reported that the oxygen vacancy can increase the carrier density of ZnO film, which also possibly influenced its electronic structure.[30] These properties were both important ETL characteristics for the perovskite solar cells.

Herein, we studied systematically the effect of different oxygen pressures on the semiconducting properties of ZnO thin films grown by PLD, which showed great influence on the photovoltaic efficiency of the $CH_3NH_3PbI_{3-x}Cl_x$-based perovskite solar cells when ZnO film was used as ETL. Such ZnO layer was substantially thinner and required no high-temperature sintering in contrast to the mesoporous TiO_2 film. Moreover, as PLD growth technique had the advantages such as the short growth cycle, less impurity, and better crystallinity, we can adjust the physical properties of ZnO ETL by controlling the growth condition like oxygen pressures. The optimized growth conditions for ZnO ETL were obtained for ZnO/$CH_3NH_3PbI_{3-x}Cl_x$/P3HT/Au planar solar cell with an efficiency of 6.3%. After further surface modification of ZnO ETL with a PCBM layer, the efficiency increased to 7.5%. These characteristics favored the development of large area flexible solar cells with a predesigned process.

2 | EXPERIMENTAL PROCEDURE

2.1 | Growth of ZnO thin films under different oxygen pressures

ZnO targets made from pressed and sintered oxide powders were adopted for PLD. KrF excimer laser (CompexPro 205, Coherent) pulses with a 10 Hz repetition frequency were applied. Fluorine-doped tin oxide (FTO)-coated glass (15 Ω/sq, Pilkington, Minato-ku, Tokyo, Japan) was used as substrate for ZnO film growth at ambient temperature. The O_2 pressure was controlled in the range of 10^{-3} Pa-10^2 Pa. The laser energy density focused on the target was about 2 J/cm^2. The distance between target and substrate was 100 mm.

2.2. | Fabrication of $CH_3NH_3PbI_{3-x}Cl_x$ perovskite solar cells

Perovskite solar cells were prepared as schematically shown in Figure 1. The devices were fabricated with the structure of FTO/ZnO/$CH_3NH_3PbI_{3-x}Cl_x$/P3HT/Au. A 70 nm ZnO layer was prepared by PLD method under different oxygen pressures. We used a mixture of $PbCl_2$ and PbI_2 as the precursor, and spin-coated at 5000 rpm on the compact ZnO film. Then, it was annealed at 70°C for 30 minute. The CH_3NH_3I solution was added onto the surface and kept for 46 seconds and spin-coated at 5000 rpm for 30 seconds to form the $CH_3NH_3PbI_{3-x}Cl_x$ film. The film color changed from chartreuse to dark brown, indicating the formation of the perovskite. Then, P3HT was coated onto the perovskite layer at 2500 rpm for 30 seconds. Finally, Au electrodes were thermally deposited under high vacuum through a shadow mask. The devices with PCBM as modified layer were fabricated on the basis of the structure of FTO/ZnO/PCBM/ $CH_3NH_3PbI_{3-x}Cl_x$/P3HT/Au. PCBM film was cast from a solution with 20 mg/mL in chlorobenzene at 3500 rpm for 30 seconds. Sample and device characterization details were presented as Supporting Information.

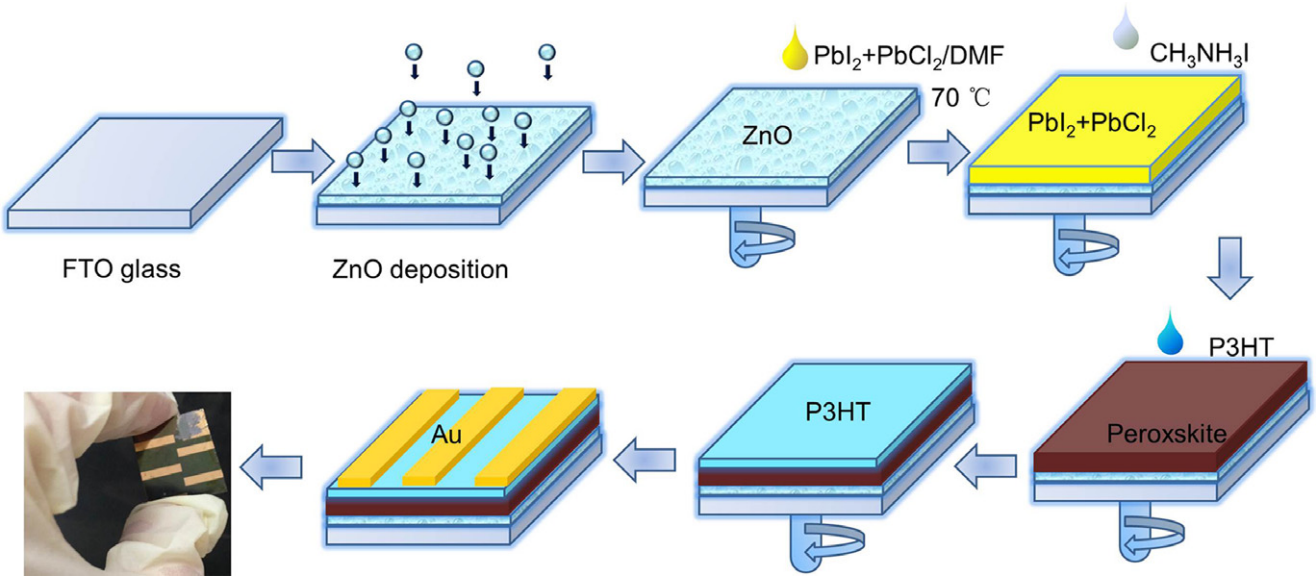

FIGURE 1 Schematic illustration of perovskite solar cells fabricated by two-step sequential deposition method [Color figure can be viewed at wileyonlinelibrary.com]

3 | RESULTS AND DISCUSSIONS

3.1 | Effect of oxygen pressure on ZnO transparent and conductive properties

When ZnO film is used as ETL, the first physical property to be checked is the optical transmittance. Figure 2 shows the typical optical photos and according transmission spectra of the ZnO films grown under different oxygen pressures, from 10^{-3} Pa to 10^{2} Pa. ZnO thin film is black when the oxygen pressure is under 10^{-3} Pa, which is due to the incomplete oxidation of Zn^{2+} ions produced by laser ablation. ZnO film under 2 Pa shows a slight yellow color.

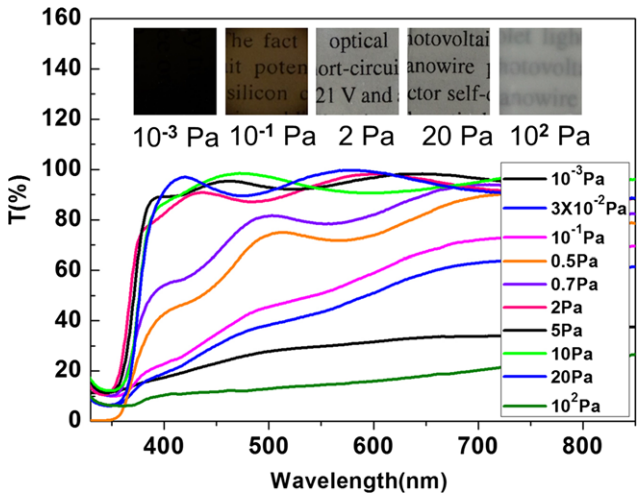

FIGURE 2 The photos of ZnO films and transmittance spectra of ZnO films prepared under different oxygen pressures (10^{-3} Pa-10^{2} Pa) [Color figure can be viewed at wileyonlinelibrary.com]

With the oxygen pressure increasing, the color is lighter and the film becomes transparent gradually. But when the oxygen pressure reaches 10^{2} Pa, the film becomes opaque due to the surface roughness. The UV/vis transmittance spectra of the ZnO samples prepared under different oxygen pressures are also shown in Figure 2. The transmittance of the sample under 10^{-3} Pa is only 30% in the visible wavelength range. With the increase of oxygen pressures in the range of 3×10^{-2} Pa-30 Pa, the transmittance of the samples become higher. Typically, all the films in the range of 2-20 Pa exhibit typical transmittance higher than 90%. But when oxygen pressure reaches 100 Pa, the crystal quality of the film reduces and a large number of particles appear on the surface. The film becomes opaque and the optical transmittance of this film suddenly drops to 20%. When ZnO film acts as ETL of the perovskite solar cell, the high optical transmittance is beneficial to improve the utilization efficiency of solar radiation. According to the transparent properties of the ZnO films, we choose the ZnO film grown under oxygen pressure of 2-20 Pa.

Resistivity (ρ) is the second physical property should be considered when ZnO film is used as ETL, which is closely related with the PLD growth conditions. Figure 3A shows an X-ray photoelectron survey spectrum (XPS) of ZnO film prepared under 10^{-1} Pa. In Figure 3B, the peaks at 1043.49 and 1020.37 eV correspond to the bonding energies (BE) of Zn2$p_{1/2}$ and Zn2$p_{3/2}$, respectively, which are attributed to Zn–O bonds.[31] Figure 3C-E are XPS spectra of O1*s* detected from ZnO films grown under different oxygen pressures. Only Zn, O, and C elements are detected, which indicates that there is no impurity in the PLD-grown ZnO film.[32] But, the Zn/O ratio is different

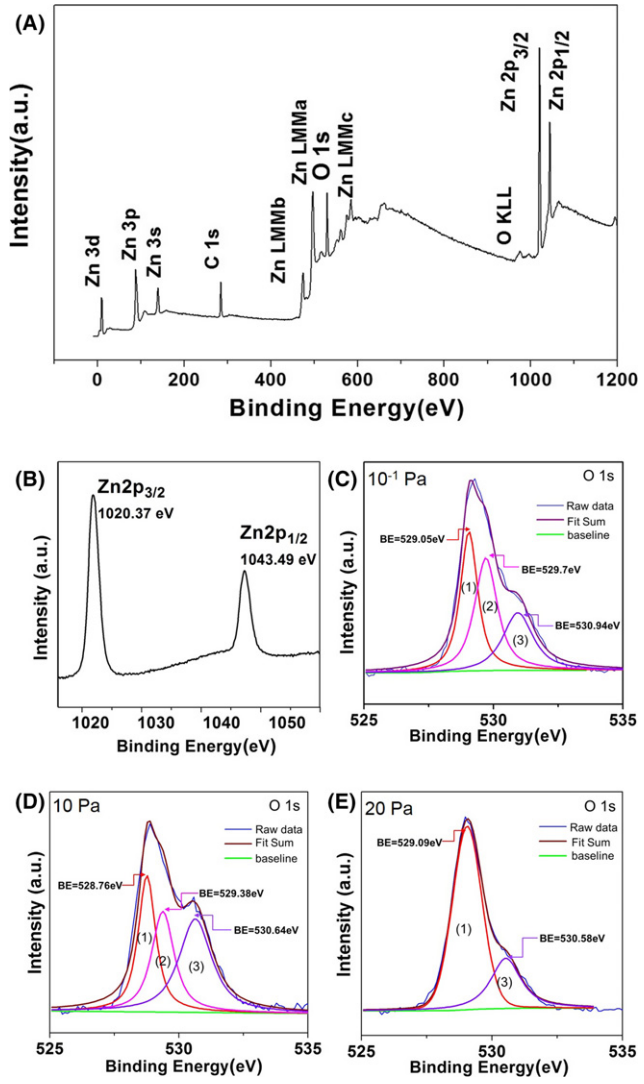

FIGURE 3 (A) X-ray photoelectron survey spectrum of ZnO film prepared under 10^{-1} Pa, (B) high-resolution X-ray photoelectron spectra of Zn2*p* of ZnO film prepared under 10^{-1} Pa, XPS spectra of O 1*s* of ZnO films under different oxygen pressures (C) 10^{-1} Pa, (D) 10 Pa, and (E) 20 Pa [Color figure can be viewed at wileyonlinelibrary.com]

TABLE 1 Summary of Zn/O ratio of ZnO films prepared under different oxygen pressures

	Zn At. (%)	O At. (%)	Zn/O ratio
0.1 Pa	52.19	47.81	1.11
10 Pa	44.39	55.61	0.78
20 Pa	46.37	53.63	0.87

when the oxygen growth pressure changes, as shown in Table 1. At low oxygen growth pressure of 10^{-1} Pa, due to the formation of oxygen vacancy (V_o) defects, the Zn/O ratio is 1.11. This can be proved by the O1*s* peak analysis. Generally, the O1*s* core-level spectrum of ZnO shows three different peaks. The Gaussian-fitted peaks marked as (1), (2), and (3) from the low BE to high BE are shown in Figure 3C-E. Peak (1) is assigned to O^{2-} ions in the Zn–O bonding of the wurtzite ZnO.[31] Peak (2) is associated with O^{2-} ions in the oxygen-deficient regions within the matrix of ZnO.[33] Peak (3) is usually due to the presence of loosely bound oxygen on the surface of ZnO films, eg, O_2.[17] The detailed composition analysis of O1*s* peak was shown in Table S1 in Supporting Information. For ZnO film of 10^{-1} Pa, a clear peak (2) from oxygen vacancy (V_o) defects was observed together with the relative weak peak (3) from bound oxygen. When the oxygen pressure increases to 10 Pa, the Zn/O ratio decreases to 0.78 as a result of decreasing Vo defects and increasing O_2. When the oxygen pressure increases to 20 Pa, the Zn/O ratio increases to 0.87. In this case, peak (2) due to V_o disappear and peak (3) also decrease. In summary, the Zn/O ratio first decreases and then increases with a turning point at growth pressure of 10 Pa.

Oxygen vacancy is one of the most important defects that affect the electrical behavior of ZnO film,[34] and the above XPS analysis can support well the Hall data shown in Figure 4, where the resistivity (ρ), carrier concentration (*n*), and carrier mobility (μ) of ZnO films are plotted as a function of oxygen pressure. As V_o indicated with peak (2) is the main n-type donor for ZnO film, the electron concentration continues to decrease from 2.2×10^{19}-7.5×10^{16} cm^{-3} when the oxygen pressures increase from 10^{-1} Pa to 20 Pa. The Hall mobility exhibits a similar turning point at 10 Pa. The first mobility decreasing is due to the increasing of adsorbed oxygen that can capture electrons, increase the grain barrier height, and scatter electrons.[35,36] When continuing to increase oxygen pressure (>10 Pa), the amount of adsorbed oxygen decreases. The following Hall mobility increase is due to the decrease of the carrier concentration.[37] The film resistivity is determined by both n and μ with $\rho = (nq\mu)^{-1}$, where *q* is the elementary charge. The films resistivity increases from 1.7×10^{-3} Ω·cm to 54 Ω·cm from 10^{-1} Pa to 20 Pa. For ZnO ETLs of the perovskite solar cell, the optimized

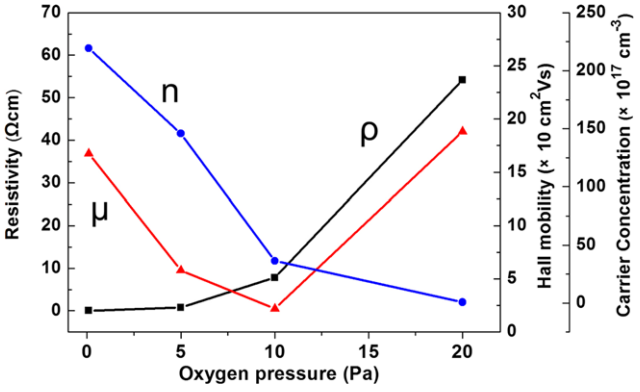

FIGURE 4 Resistivity, carrier concentration, and carrier mobility of ZnO thin films as a function of oxygen pressure, ρ represent the resistivity, *n* represent carrier concentration, μ represent hall mobility [Color figure can be viewed at wileyonlinelibrary.com]

oxygen pressure is around 5-10 Pa in terms of both resistivity and transmittance.

3.2 | Planar perovskite solar cells with different ZnO films as ETLs

Figure 5A,C,E illustrate the plan-view images of individual ZnO, perovskite and P3HT layers, respectively. The cross-sectional SEM image of the as-deposited ZnO film is clearly illustrated in Figure 5B and the film thickness is about 70 nm. As shown in Figure 5C, the average grain of the spin-coated perovskite layer is found to be ~200 nm, and the thickness is about 400 nm. It is noteworthy that the precursor materials, eg, Cl doped-PbI_2 and CH_3NH_3I, partially react with each other during the spin coating process, particularly at the interfaces between PbI_2 and CH_3NH_3I. The as-prepared $CH_3NH_3PbI_3$ films are initially yellowish-brown in color and subsequently change to dark brown. A small molecule organic polymer P3HT layer can be observed in Figure 5E. Figure 5F shows the typical cross-sectional SEM image of the planar perovskite solar cell with the following layered structure: FTO/ZnO /perovskite absorber/ P3HT/Au.

Figure 6A shows the steady-state PL spectrum of intrinsic ZnO film measured at room temperature with a 313 nm

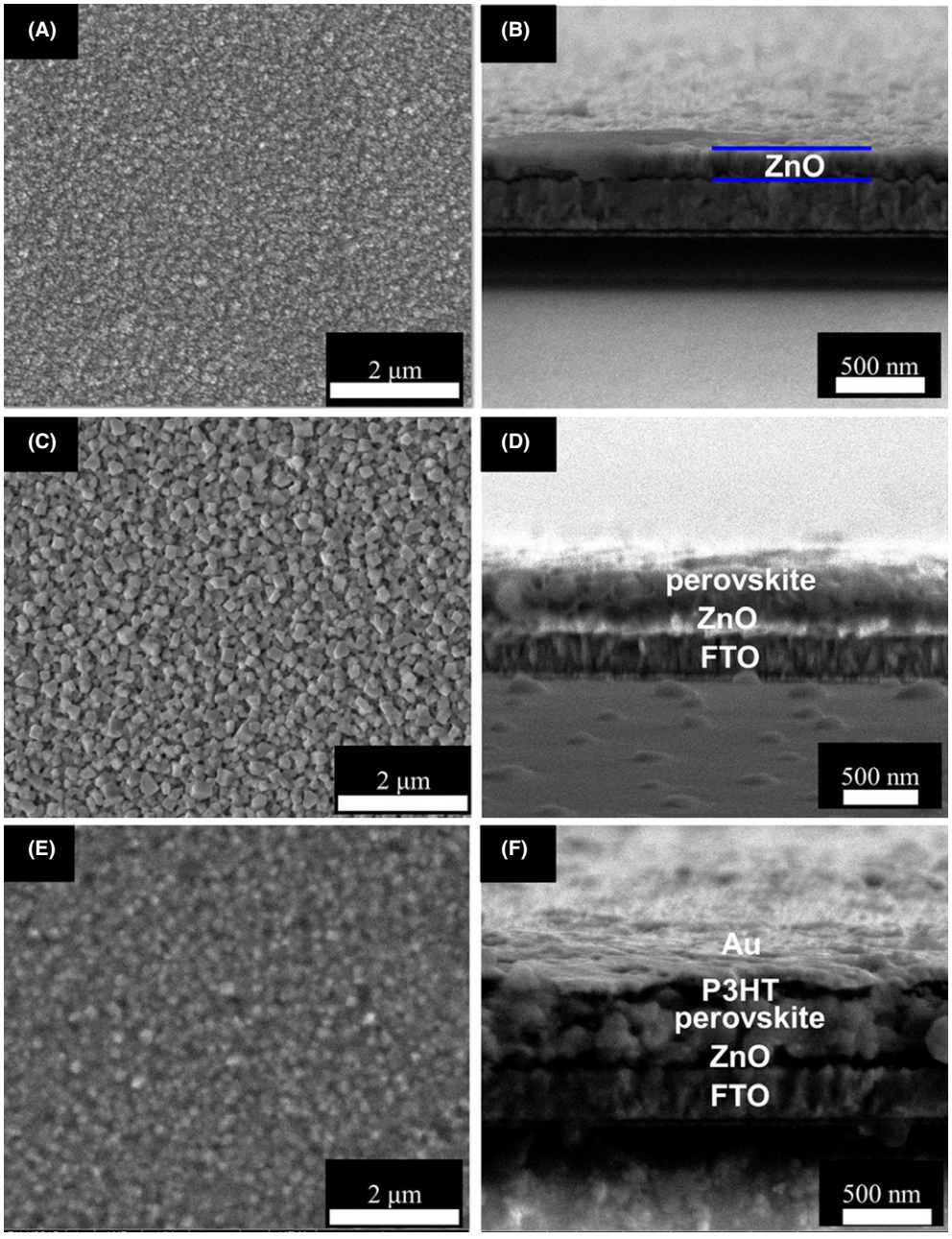

FIGURE 5 Surface cross-sectional scanning electron microscopy images of every layer of the device. (A)-(B) surface (left) and cross-sectional (right) SEM images of ZnO layer, (C)-(D) surface (left) and cross-sectional (right) SEM images of ZnO/$CH_3NH_3PbI_{3-x}Cl_x$, (E) surface SEM image of P3HT layer, (F) cross-sectional SEM image of the device [Color figure can be viewed at wileyonlinelibrary.com]

excitation light. For intrinsic ZnO sample, a sharp PL peak appears in the UV region centered around 380 nm, which is attributed to a near-band-edge recombination.[38,39] For mixed halide perovskites $CH_3NH_3PbI_{3-x}Cl_x$ sample, we adopt 450 nm light from diode laser as the excitation source. It is noted that the emission peak for the solution-processed $CH_3NH_3PbI_{3-x}Cl_x$ film is located at 767 nm with the calculated optical band gap of about 1.61 eV. The glass substrate and PbI_2 film have no emission peak in this position. Optical absorption spectra were measured on ZnO film, Cl-doped PbI_2 film and perovskite film, respectively, as shown in Figure 6B. The absorption spectrum of the ZnO layer exhibits an absorption edge at 380 nm, which corresponds to its band gap absorption.[9] The adsorption edge of the Cl-doped PbI_2 locates at about 450 nm. Compared with that of pure PbI_2 film (~520 nm),[40] the absorption edge shifts to a higher energy direction. This is mainly because Cl doping widens band gap of PbI_2 film. The optical absorption onset of the $CH_3NH_3PbI_{3-x}Cl_x$ perovskite film occurs at about 770 nm,[41] consistent with the PL data with a Stocks shift.[42] The Raman spectra were further measured under excitation with 532 nm laser for Cl-doped PbI_2 film and mixed-halide perovskite $CH_3NH_3PbI_{3-x}Cl_x$ on ZnO layer. For the Raman spectrum of Cl-doped PbI_2 film (black line), only one peak at lower frequency of 60 cm^{-1} assigned to the bending mode of the Pb–I bond is observed.[43] For mixed-halide perovskite $CH_3NH_3PbI_{3-x}Cl_x$ film, four perovskite-related peaks are observed, which are in good agreement with the density functional theory calculation.[44] The peaks at 51 and 71 cm^{-1} are assigned to the inorganic component of $CH_3NH_3PbI_{3-x}Cl_x$. The feature peaks at 110 and 167 cm^{-1} are assigned to the vibration of the MA cations.[42] However, the bands at 95 cm^{-1} is attributed to the symmetric stretch A_{1g} of PbI_2 crystal,[45,46] which is due to the degradation of $CH_3NH_3PbI_{3-x}Cl_x$ film under strong laser illumination.

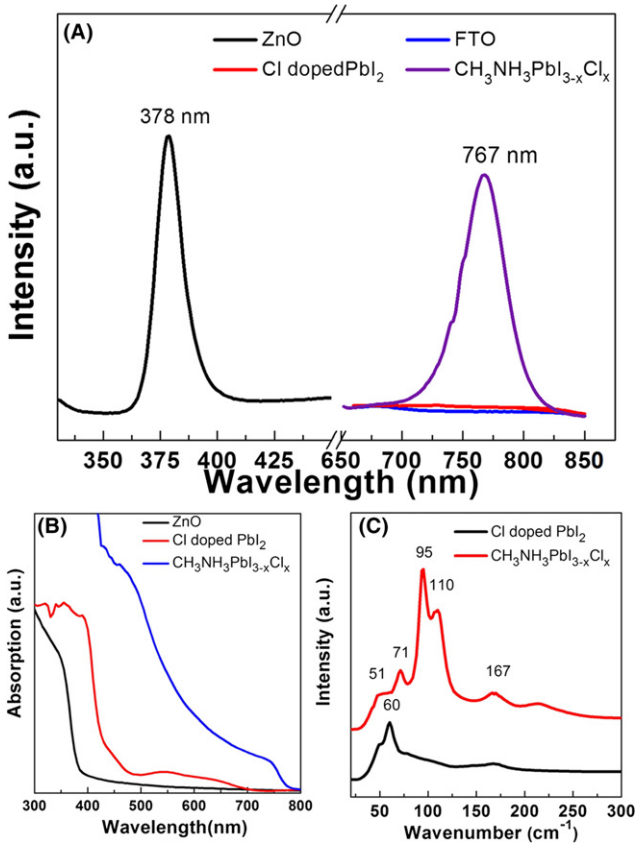

FIGURE 6 (A) Steady-state PL spectrum of ZnO film and FTO glass, Cl-doped PbI_2, $CH_3NH_3PbI_{3-x}Cl_x$ samples excitated by 313 and 450 nm light, respectively, (B) UV-vis spectra of ZnO, Cl-doped PbI_2 film and $CH_3NH_3PbI_{3-x}Cl_x$ sample, (C) Raman scattering spectra of ZnO, Cl-doped PbI_2 film and $CH_3NH_3PbI_{3-x}Cl_x$ perovskite absorber under the excitation source of 532 nm [Color figure can be viewed at wileyonlinelibrary.com]

To investigate the influence of transparent and conductive properties of ZnO films on the photovoltaic performance of according solar cells, the *J-V* curves of the ZnO/$CH_3NH_3PbI_{3-x}Cl_x$/P3HT/Au heterojunction cells are measured as shown in Figure 7. The device parameters are summarized in Table 2. The device with ZnO film grown at 10^{-3} Pa as ETL exhibits a J_{sc} = 5.79 mA/cm^2, a V_{oc} = 0.83 V, a FF = 49.68, and a PCE = 2.4%. With the oxygen pressure for ZnO film increasing from 10^{-3} Pa to 5 Pa, all of the device characteristics like V_{oc}, J_{sc}, and PCE improve obviously. The device has V_{oc} = 1.04 V, J_{sc} = 12.50 mA/cm^2, FF = 47.96%, and PCE = 6.3% with ZnO film grown at 5 Pa. Further increases in the oxygen pressures of ZnO film from 10 Pa to 10^2 Pa result in some deterioration on device performance. The measured *J-V* characteristics show close relation to the transparent and conductive properties of ZnO films. With increase of oxygen pressures from 10^{-3} Pa to 5 Pa, the surface of ZnO film become denser and smoother. Also, the crystal quality of ZnO film improves greatly. So, the V_{oc} and J_{sc} improve because of reduced photocarriers recombination. The high optical transmittance is beneficial to improve the utilization efficiency of solar radiation and will enhance the solar cell PCE. The FF value is associated with conductive property of ZnO film. When the oxygen pressure varies from 10^{-1} Pa to 5 Pa, FF values are almost similar due to the similar value of resistance observed in Figure 4. As expected, the ZnO layers obtained at the oxygen pressure of 5 Pa show significant enhancements for both V_{oc} and J_{sc} values compared to the 10^{-3} Pa sample. However, when continuing to increase oxygen pressures (10 Pa-10^2 Pa), the transparent and conductive properties of ZnO films deteriorate. So, no device performance improvements are observed when the oxygen pressure further increases from 10 Pa to 10^2 Pa.

For a high-efficiency solar cell, except active material itself, device structure and interface are also key factors. In order to modify the interface between ZnO ETL and the perovskite absorber, a PCBM layer is introduced. PCBM is

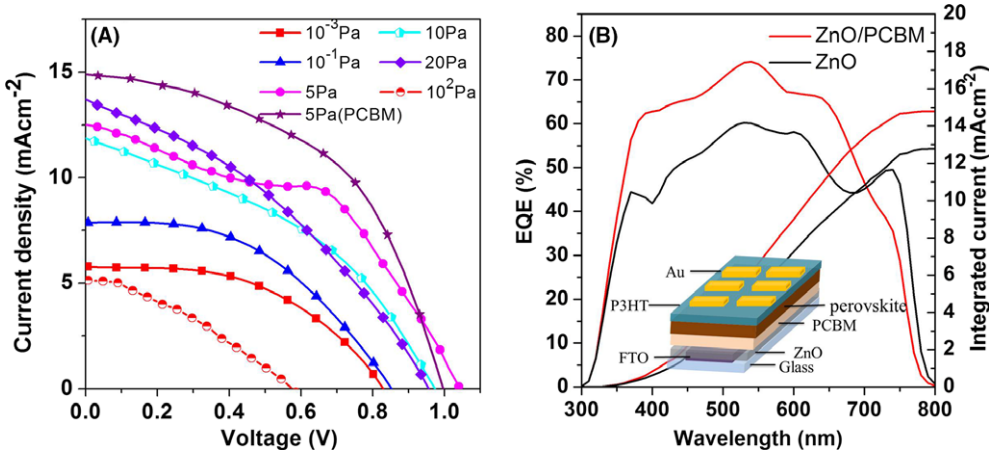

FIGURE 7 (A) The photocurrent density-voltage (*J-V*) curves of perovskite solar cells based on PLD-ZnO films, (B) external quantum efficiency (EQE) for the best cell using nanostructured ZnO film and ZnO/PCBM, inset is the schematic diagram of the cell device [Color figure can be viewed at wileyonlinelibrary.com]

TABLE 2 Photovoltaic parameters of the PLD-ZnO-based perovskite solar cells as a function of oxygen pressure

Buffer layer	V_{oc} (V)	J_{sc} (mA/cm^2)	FF (%)	PCE (%)
10^{-3} Pa (ZnO)	0.83	5.79	49.68	2.4
10^{-1} Pa (ZnO)	0.85	7.86	47.56	3.2
5 Pa (ZnO)	1.04	12.50	47.96	6.3
5 Pa (ZnO/PCBM)	1.0	14.89	50.21	7.5
10 Pa (ZnO)	0.97	11.86	39.57	4.6
20 Pa (ZnO)	0.97	13.75	36.49	4.9
10^2 Pa (ZnO)	0.58	5.22	33.29	1.1

a typical fullerene derivative with good solubility and high electron mobility and has become a standard for organic solar cell electron acceptor. PCBM, as an interface modifier, can combine closely with both the ZnO layer and the absorption layer. Interface modification can help relatively fast extract free electrons and, therefore, enhance the cell performance. After interface modification, the perovskite solar cell exhibits higher characteristic data, eg, V_{oc} = 1.0 V, J_{sc} = 14.89 mA/cm^2, FF = 50.21%, and PCE = 7.5%. Figure 7B compares the external quantum efficiency (EQE) spectra from 300 to 800 nm measured from perovskite solar cells with and without PCBM interlayer. With PCBM layer, EQE in almost the whole visible wavelength region is enhanced, thus leading to a clear improvement in J_{SC}. The integrated photocurrent densities are 14.78 and 12.7 mA/cm^2 corresponding to the solar cells with ZnO and ZnO/PCBM layers, respectively, in good agreement with the experimental results in Table 2. The photo-induced free carriers must transfer across the interfaces to be collected, and the charge recombination usually occurs at the interfaces due to interfacial defects.[10] So, introducing a PCBM layer plays an important role in suppressing charge recombination.

4 | CONCLUSION

In summary, we have a detailed research about precisely controlling the semiconductor property of ZnO film like transparency and conductivity that is very important for PSC performance. The photovoltaic performance is explored using a P–i–N solar cell with a ZnO/$CH_3NH_3PbI_{3-x}Cl_x$/P3HT/Au configuration, where PLD grown ZnO film acts as ETL. The best-performing device exhibits a PCE of 6.3% when ZnO ETL is prepared under 5 Pa. When PCBM is further introduced into the solar cell as interface modifier, the PCE was further increased to 7.5%. The high optical transmittance is beneficial to improve the utilization efficiency of solar radiation and the better conductive property of ZnO film is associated with higher FF. So, regulating transparent and conductive properties of ZnO films by controlling the oxygen pressure is essential for developing perovskite solar cells.

ACKNOWLEDGMENTS

This work is supported by NSFC (51472110, 11174112) and Shandong Provincial Natural Science Foundation (JQ201214, 2014ZRB01A47). The research program from Ministry of Education, China, is also acknowledged (213021A). BC thanks the Taishan Scholar Professorship tenured at University of Jinan and the postgraduate innovation project (YCXB15001) from the University.

REFERENCES

1. Cheng YH, Yang QD, Xiao JY, et al. Decomposition of organometal halide perovskite films on zinc oxide nanoparticles. *ACS Appl Mater Interfaces*. 2015;7:19986–19993.
2. Kim HS, Im SH, Park NG. Organolead halide perovskite: New horizons in solar cell research. *J Phys Chem C*. 2014;118(11):5615–5625.

3. Snaith HJ. Perovskites: The emergence of a new era for low-cost, high efficiency solar cells. *J Phys Chem Lett*. 2013;4:3623–3630.
4. Liu MZ, Johnston MB, Snaith HJ. Efficient planar heterojunction perovskite solar cells by vapour deposition. *Nature*. 2013;501(19):395–398.
5. Chen Q, Zhou HP, Hong ZR, et al. Planar heterojunction perovskite solar cells via vapor-assisted solution process. *J Am Chem Soc*. 2014;136 (2):622–625.
6. Im JH, Jang IH, Pellet N, Graetzel M, Park NG. Growth of $CH_3NH_3PbI_3$ cuboids with controlled size for high-efficiency perovskite solar cells. *Nat Nanotechnol*. 2014;9:927–932.
7. Nie W, Tsai H, Asadpour R, et al. High-efficiency solution-processed perovskite solar cells with millimeter-scale grains. *Science*. 2015;347:522–525.
8. Heo JH, Han HJ, Kim D, Ahn TK, Im SH. Hysteresisless inverted $CH_3NH_3PbI_3$ planar perovskite hybrid solar cells with 18.1% power conversion efficiency. *Energy Environ Sci*. 2015;8:1602–1608.
9. Juarez-Perez EJ, Wuβler M, Fabregat-Santiago F, et al. Role of the selective contacts in the performance of lead halide perovskite solar cells. *J Phys Chem Lett*. 2014;5:680–685.
10. Shi JJ, Xu X, Li DM, Meng QB. Interfaces in perovskite solar cells. *Small*. 2015;11(21):2472–2486.
11. Xing GC, Mathews N, Sun SY, et al. Long-range balanced electron-and hole-transport lengths in organic-inorganic $CH_3NH_3PbI_3$. *Science*. 2013;342:344–347.
12. Stranks SD, Eperon GE, Grancini G, et al. Electron-hole diffusion lengths exceeding 1 micrometer in an organometal trihalide perovskite absorber. *Science*. 2013;342:341–344.
13. Kim J, Kim G, Kim TK, et al. Efficient planar-heterojunction perovskite solar cells achieved via interfacial modification of a sol-gel ZnO electron collection layer. *J Mater Chem A*. 2014;2:17291–17296.
14. Dong X, Hu H, Lin B, Ding J, Yuan N. The effect of ALD-ZnO layers on the formation of $CH_3NH_3PbI_3$ with different perovskite precursors and sintering temperatures. *Chem Commun*. 2014;50:14405–14408.
15. Bi DQ, Tress W, Dar MI, et al. Efficient luminescent solar cells based on tailored mixed-cation perovskites. *Sci Adv*. 2016;2(1):1501170.
16. Zhang QF, Dandeneau CS, Zhou XY, Cao GZ. ZnO nanostructures for dye-sensitized solar cells. *Adv Mater*. 2009;21:4087–4108.
17. Hu XL, Gong HB, Xu HY, et al. Influences of target and liquid media on morphologies and optical properties of ZnO nanoparticles prepared by laser ablation in solution. *J Am Chem Soc*. 2011;94(12):4305–4309.
18. Li H, Zhang Y, Wang J. ZnO nanosheets derived from surfactant-directed process: growth mechanism, and application in dye-sensitized solar cells. *J Am Chem Soc*. 2012;95(4):1241–1246.
19. Liu D, Gangishetty MK, Kelly TL. Effect of $CH_3NH_3PbI_3$ thickness on device efficiency in planar heterojunction perovskite solar cells. *J Mater Chem A*. 2014;2:19873–19881.
20. Liu D, Yang J, Kelly TL. Compact layer free perovskite solar cells with 13.5% efficiency. *J Am Chem Soc*. 2014;136(49):17116–17122.
21. Son DY, Im JH, Kim HS, Park NG. 11% efficient perovskite solar cell based on ZnO nanorods: An effective charge collection system. *J Phys Chem C*. 2014;118:16567–16573.
22. Liu D, Kelly TL. Perovskite solar cells with a planar heterojunction structure prepared using room-temperature solution processing techniques. *Nature Photon*. 2014;8:133–138.
23. Mahmood K, Swain BS, Amassian A. Double-layered ZnO nanostructures for efficient perovskite solar cells. *Nanoscale*. 2014;6:14674–14678.
24. Song JX, Bian J, Zheng EQ, Wang XF, Tian WJ, Miyasaka T. Efficient and environmentally stable perovskite solar cells based on ZnO electron collection layer. *Chem Lett*. 2015;44:610–612.
25. Tseng ZL, Chiang CH, Wu CG. Surface engineering of ZnO thin film for high efficiency planar perovskite solar cells. *Sci Rep*. 2015;5:13211–13220.
26. Liu ZW, Ong CK. Synthesis and size control of ZnO nanorods by conventional pulsed-laser deposition without catalys. *Mater Lett*. 2007;61 (16):3329–3333.
27. Lin SS, Hong JI, Song JH, et al. Phosphorus doped $Zn_{1-x}Mg_xO$ nanowire arrays. *Nano Lett*. 2009;9(11):3877–3882.
28. Cao BQ, Pérez JZ, Czekalla C, et al. Tuning the lateral density of ZnO nanowire arrays and its application as physical templates for radial nanowire heterostructures. *J Mater Chem*. 2010;20:3848–3854.
29. Carcia PF, McLean RS, Reilly MH, Nunes G. Transparent ZnO thin-film transistor fabricated by rf magnetron sputtering. *Appl Phys Lett*. 2003;82:1117–1119.
30. Hausmann A, Utsch B. Oxygen ion vacancies as donors in zinc-oxide. *Zeitschrift fur Physik B-Condensed Matter*. 1975;21(3):217–220.
31. Das J, Pradhan SK, Sahu DR, et al. Micro-raman and XPS studies of pure ZnO ceramics. *Phys B*. 2010;405:2492–2497.
32. Wagner CD, Gale LH, Raymond RH. Two-dimensional chemical state plots: a standardized data set for use in identifying chemical states by X-ray photoelectron spectroscopy. *Anal Chem*. 1979;51:466–482.
33. Du Y, Zhang MS, Hong J, Shen Y, Chen Q, Yin Z. Structural and optical properties of nanophase zinc oxide. *Appl Phys A*. 2003;76:171–176.
34. Cao BQ, Cai WP, Zeng HB. Temperature-dependent shifts of three emission bands for ZnO nanoneedle arrays. *Appl Phys Lett*. 2006;88:161101–161103.
35. Klingshim CF, Meyer BK, Waag A, Hoffillann A, Geurts J. *Zinc Oxide: From fundamental Properties Towards Novel Applications*. NewYork, NY: Springer; 2010:104–105.
36. Dong J, Zhao Y, Shi J, et al. Impressive enhancement in the cell performance of ZnO nanorod-based perovskite solar cells with Al doped ZnO interfacial modification. *Chem Commun*. 2014;50:13381–13384.
37. Kim DH, Cho NG, Kim HG, Choi WY. Structural and eleetrical Properties of indium doped ZnO thin films fabricated by RF magnetron sputtering. *J Electrocheln Soc*. 2007;154:939–943.
38. Qiu ZW, Yang XP, Han J, et al. Sodium-doped ZnO nanowires grown by high-pressure PLD and their acceptor-related optical properties. *J Am Chem Soc*. 2014;97(7):2177–2184.
39. Guzmán Embús DA, Vargas Charry MF, Vargas Hernández C. Optical and structural properties of ZnO and ZnO: Cd particles grown by the hydrothermal method. *J Am Chem Soc*. 2015;98:1498–1505.
40. Lee MM, Teuscher J, Miyasaka T, Murakami TN, Snaith HJ. Efficient hybrid solar cells based on meso-superstructured organometal halide perovskites. *Science*. 2012;338:643–647.
41. Qin P, Tetreault N, Dar MI, et al. A novel oligomer as a hole transporting material for efficient perovskite solar cells. *Adv Energy Mater*. 2014;5:1400980–1400984.
42. Quarti C, Grancini G, Mosconi E, et al. The raman spectrum of the $CH_3NH_3PbI_3$ hybrid perovskite: Interplay of theory and experiment. *J Phys Chem Lett*. 2014;5:279–284.
43. Preda N, Mihut L, Baibarac M, Husanu M, Bucur C, Baltog I. Raman and photoluminescence studies on intercalated lead iodide with pyridine and iodine. *J Optoelectron Adv Mater*. 2008;10:319–322.
44. Park BW, Jain SM, Zhang XL, Hagfeldt A, Boschloo G, Edvinsson T. Resonance raman and excitation energy dependent charge transfer mechanism in halide-substituted hybrid perovskite solar cells. *ACS Nano*. 2015;9 (2):2088–2101.
45. Nakashima S. Raman study of polytypism in vapor-grown PbI_2. *Solid State Commun*. 1975;16:1059–1062.

46. Capozzi V, Fontana A, Fontana M, Mariotto G, Montagna M, Viliani G. Raman-scattering in PbI_2. *Il Nuovo Cimento B*. 1977;39:556–568.

SUPPORTING INFORMATION

Additional Supporting Information may be found online in the supporting information tab for this article.

How to cite this article: Qiu Z, Yuan S, Gong H, et al. The influence of physical properties of ZnO films on the efficiency of planar ZnO/perovskite/P3HT solar cell. *J Am Ceram Soc*. 2017;100:176–184. doi: 10.1111/jace.14491.